# Graphene quantum dots: Beyond a Dirac billiard

Florian Libisch,[1] Christoph Stampfer,[2] and Joachim Burgdörfer[1]
[1]*Institute for Theoretical Physics, Vienna University of Technology, Wiedner Hauptstraße 8-10/136, A-1040 Vienna, Austria, European Union*
[2]*Solid State Physics Laboratory, ETH Zurich, 8093 Zurich, Switzerland*
(Received 20 August 2008; published 17 March 2009)

We present realistic simulations of quantum confinement effects in phase-coherent graphene quantum dots with linear dimensions of 10–40 nm. We determine wave functions and energy-level statistics in the presence of disorder resulting from edge roughness, charge impurities, or short-ranged scatterers. Marked deviations from a simple Dirac billiard for massless fermions are found. We find a remarkably stable dependence of the nearest-neighbor level spacing on edge roughness suggesting that the roughness of fabricated devices can be possibly characterized by the distribution of measured Coulomb blockade peaks.

DOI: 10.1103/PhysRevB.79.115423 PACS number(s): 73.22.Dj, 05.45.Mt, 73.23.−b, 81.05.Uw

## I. INTRODUCTION

Graphene,[1,2] the first true two-dimensional (2D) solid, is attracting considerable attention, mostly due to unique dynamics of electrons near the Fermi energy which closely mimics that of a massless Dirac Hamiltonian [see Fig. 1(a)]. Moreover, the double cone structure near the $K$ and $K'$ points of the sublattices in reciprocal space gives rise to a "pseudospin" degeneracy, suggesting an analogy to Dirac four spinors. Envisioned applications range from high-mobility nanoelectronics,[3] spin qubits in graphene quantum dots,[4] and the creation of "neutrino" billiards.[5,6] Dirac (including neutrino) billiards receive growing interest as a complement to classical and quantum (Schrödinger) billiards, which have taken central stage in studies elucidating the quantum-to-classical crossover in both regular and chaotic devices. Quantum billiards are the paradigm for simple Hamiltonian systems featuring complex dynamics.[7] Additionally, spin coherence times in graphene are expected to be very long due to weak spin-orbit and hyperfine couplings[8–10] making graphene quantum dots a promising candidate for future spin based quantum information processing.[4] However, confining electrons in graphene is a challenge due to the gapless electronic structure and the Klein tunneling paradox.[11,12] This difficulty has recently been overcome by structuring 2D graphene, and certain quantum-mechanical confinement effects have been observed in nanoribbons,[13–18] interference devices,[19] single electron transistors,[3,20,21] and graphene quantum dots.[6,22]

In the following we present realistic simulations for single-particle spectra of graphene quantum dots (i.e., billiards) by explicitly considering rough edges and disorder. This work was motivated by recent advances in fabricating dots with linear dimension $d$ ranging from a few hundred nanometers down to about 40 nm, and determining their nearest-neighbor energy-level spacing distribution.[6,21] We analyze dot wave functions, the density of states (DOS), and the nearest-neighbor spacing distribution (NNSD). We address the question to what extent the electron spectra now experimentally accessible via measurements of Coulomb blockade peaks reveal information on the roughness and size of the graphene quantum dot. To put it provocatively: Can one "hear" the rugged shape of a drum if it is made of a graphene flake?

## II. METHOD

We investigate graphene dots with linear dimensions between 10 and 40 nm, containing between 6000 and 75 000 carbon atoms. This size agrees with currently fabricated devices.[6] The shape is chosen to represent a classically regular structure in the absence of edge roughness. One motivation of this choice was the remarkable result[5] that a Dirac neutrino billiard, in sharp contrast to a Schrödinger billiard, would feature chaotic dynamics. We neglect inelastic scattering inside the dot. This is justified as the inelastic mean-free path $\lambda_{il}$ found in experiment exceeds the linear dimension $d \ll \lambda_{il} \approx 400$ nm.[1] Our simulation allows for the inclusion of disorder through (i) edge roughness [see Fig. 1(c)], (ii) short-range disorder due to randomly distributed point defects in the interior, and (iii) long-range screened Coulomb distortion due to charge deposition in either the substrate or the flake. Rough edges are simulated by modulating the boundary of the dot by steps of height $\pm\delta w$ and length $\pm\delta l$ randomly chosen from the interval $[0,\Delta W]$, $\Delta W \ll d$. We refer to $\Delta W$ as the amplitude of edge roughness which varies between 0.3 (weak disorder) and 2 nm (strong disorder). The resulting piecewise straight edge features alternating zigzag and armchair sections [see Figs. 1(b) and 1(c)]. We describe impuri-

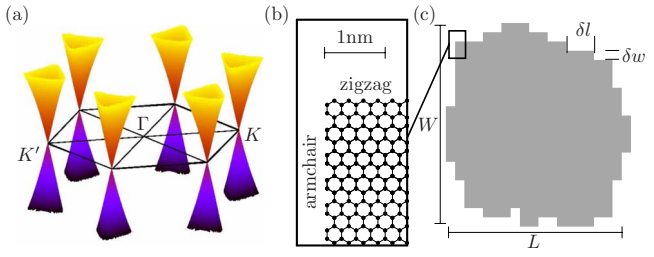


FIG. 1. (Color online) (a) Graphene dispersion near $K$ and $K'$ points of the infinitely extended sheet. (b) Rectangular segment of a graphene flake, vertical edge armchair, and horizontal edge zigzag terminated. (c) (Approximately) rectangular quantum dot with rough edges.

 

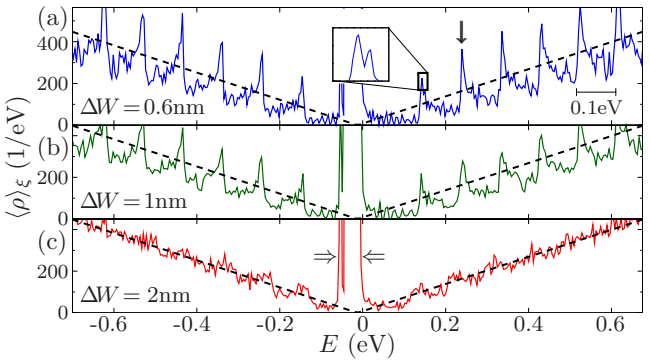


FIG. 2. (Color online) Ensemble-averaged density of states $\langle\rho(E)\rangle_\xi$ of graphene quantum dots with increasing edge roughness, see different values for $\Delta W$ in the subfigures. The size of all devices is equal, $d=20$ nm (20 000 atoms) and their width $W=16$ nm. Dashed lines indicate the averaged linear DOS for Dirac billiards [see Eq. (1)]. The inset shows the $K-K'$ splitting of 12 meV.

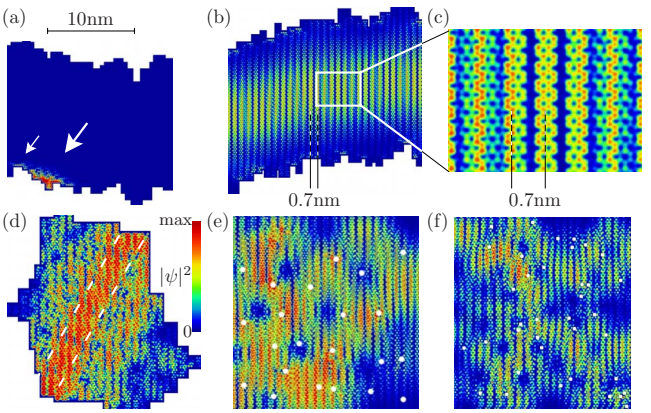


FIG. 3. (Color online) Eigenstates of graphene quantum dots with dot area of about 225 nm$^2$ (13 000 carbon atoms, fewer than in Fig. 2, for demonstration purposes only). Eigenenergies are (a) 65, [(b) and (c)] 220, (d) 650, (e) 300, and (f) 1020 meV, respectively. Eigenstates for edge roughness [at constant $\Delta W=1$ nm, (a)–(c)], short-range impurities [$n_D=0.003$ in (e), white dots mark the impurity center], and long-range impurities [$n_C=0.005$ in (e)] are shown.

ties and defects in the flake by positioning either long-range $[V(\mathbf{r})=V_0e^{-\alpha|\mathbf{r}-\mathbf{r}_0|}]$, with $\alpha^{-1}$ larger than the lattice spacing, or short-range $[V(\mathbf{r})=\delta(\mathbf{r}-\mathbf{r}_0)]$ scatterers at randomly selected lattice sites $\mathbf{r}_0$. We use impurity densities for short-range ($n_D$) and long-range ($n_C$) scatterers of $n_i<1.8\times10^{-3}$ impurities/carbon (10–100 defects per flake), as estimated by recent work.[23]

The spectrum of the graphene quantum dots is determined by employing a Lanczos algorithm[24] giving the 500 eigenstates closest to the Fermi edge. The graphene flake is described by a third nearest-neighbor tight-binding approximation to correctly reproduce the graphene band structure.[25] The modified C-C bond length at the flake boundary is accounted for by increasing nearest-neighbor coupling to the outmost carbon atoms by 12% in accordance with recent *ab initio* density-functional calculations.[26] Our ensemble averages for the DOS $\langle\rho\rangle_\xi=\langle\Sigma_i\delta(E-E_i)\rangle_\xi$ encompass typically 5000 disorder realizations $\xi$.

## III. DENSITY OF STATES

The linear dispersion relation of a massless Dirac particle implies a DOS linear in $\varepsilon$,

$$\rho(\varepsilon)=\frac{1}{2(\hbar v_F)^2}d^2|\varepsilon|, \tag{1}$$

where $d=\sqrt{4WL/\pi}$ is the effective diameter of a dot with area $WL$ and $\varepsilon$ is measured relative to the conical intersection [Fig. 1(a)] assumed to coincide with the Fermi edge. The simulated DOS for the quantum dots display marked deviations from Eq. (1). For weak disorder pronounced size quantization peaks appear [see, e.g., vertical arrow in Fig. 2(a)]. Their positions are determined by the smallest linear dimension of the flake.[27] We have investigated both cases $W<L$ ($W>L$), and find the same qualitative behavior. In the following, we assume $W<L$. Note that width ($W$) and length ($L$) of the rectangular flake are not strictly equivalent as the vertical boundary features an arm-chair border while the horizontal forms a zigzag border. The distance between the size quantization peaks is $\Delta E=\hbar v_F\pi/W\approx1.5/W$[eV], with the width $W$ given in nanometer. This yields a prediction for the energy separation of 0.1 eV for the peaks in Fig. 2. Weak disorder, i.e., small edge roughness, can induce coupling between the cones at $K$ and $K'$ [Fig. 1(a)]. This manifests itself by a fine structure of size quantization peaks by lifting the degeneracy [inset of Fig. 2(a)]. The quantum confinement peaks in the graphene dot are enhanced compared to a corresponding Schrödinger billiard of the same geometry in part because of both the altered dispersion relation and the additional degeneracy. Strong edge disorder smears out size quantization patterns and the DOS begins to resemble that of a zero-mass Dirac fermion in free space [Eq. (1)]. Only when the edge roughness can be limited to the subnanometer scale does quantized conductance in graphene nanoribbons persist.[15]

Even in the limit of strong disorder, the prominent peak in the DOS near the Fermi edge remains unchanged [see horizontal arrows in Fig. 2(c)]. A direct look at the wave function [Fig. 3(a)] reveals its origin: a large number of strongly localized states at the zigzag edges of the graphene flake. Surface states at the zigzag edges are well known from transport through graphene nanoribbons.[28] The additional inclusion of edge roughness leads to exponential (Anderson-type) localization along the flake boundary, as a fit to our data confirms (not shown): each eigenstate features a nonvanishing amplitude only at a few (not always spatially connected) carbon atoms, with a decay length into the bulk of typically 0.5 nm [see arrows in Fig. 3(a)]. A similar effect was observed in transport, where edge roughness leads to Anderson localization in scattering states.[29] In contrast, for straight zigzag edges (i.e., no edge disorder) eigenstates extend over many lattice constants along the flake boundary without localization parallel to the edges. We find that the eigenenergies of localized states are extremely sensitive to the site energies at the corresponding lattice sites. This agrees well with the experimental observations of sharp resonance in the electron

transport through graphene constrictions.[20] We expect that different functional groups (e.g., H– or OH–) attached to the outermost carbon atoms may strongly influence the local DOS and the position of this localization peak relative to the Fermi edge.

Delocalized states contributing to the size quantization peaks show pronounced features well beyond the simple picture of a confined zero-mass Dirac particle. While the transverse quantization resembles that of a conventional conductor, the interference pattern in the electron probability density $|\psi|^2$ [Fig. 3(b)] results from the simultaneous presence of multiple wavelength scales for the cone near the $K$ point (unlike wave functions near the $\Gamma$ point) in $\mathbf{k}=(k_0+v_F\pi/L, v_F\pi/W)$: parallel to armchair edges (i.e., in vertical direction in Fig. 3), the wavelength is of the order of twice the width of the ribbonlike dot $\approx 32$ nm. Parallel to zigzag edges (i.e., in horizontal direction in Fig. 3), the wave oscillations are much shorter with a typical wavelength of 0.7 nm [see Fig. 3(c)] resulting from beating (frequency ratio 3:2) between lattice periodicity $a=0.24$ nm and the characteristic wavelength $\lambda_0=2\pi/k_0\approx 0.37$ nm, where $k_0 \gg v_F\pi/L$ is the distance between $\Gamma$ and $K$ points in reciprocal space [see Fig. 1(a)]. We find beating patterns with this characteristic length scale to be universally present in all delocalized states, even in the presence of long-range disorder. Only because of the subnanometer length scale of $\lambda_0$ at the $K$ point is the graphene dot sensitive to edge roughness and disorder on a length scale of a few nanometers, in contrast to a Dirac cone at the $\Gamma$ point. In momentum space, the wave function for the lowest transverse quantum number shown in Fig. 3(b) is displaced relative to the $K$ point $(k_0,0)$ in $k_x$ direction [as opposed to the directions rotated by 60° and 120°, $\frac{1}{2}(k_0, \pm\sqrt{3}k_0)$, see Fig. 1(a)] because of the alignment of the zigzag (armchair) edges parallel (orthogonal) to the $(k_0,0)$ direction. However, all three directions appear for higher transverse quantum numbers, resulting in enhancements along the three zigzag directions of the lattice [i.e., horizontal, 60°, and 120°, see dashed lines in Fig. 3(c)]. As a consequence, eigenstates feature a 2D hole ("swiss-cheese") pattern emerging from the interference of plane waves rotated by 60° relative to each other [see Figs. 3(e) and 3(f)].

## IV. NEAREST NEIGHBOR SPACING DISTRIBUTION

In order to delineate the influence of disorder and edge roughness on the energy-level statistics, we have determined the NNSD, $P(\Delta E)$, i.e., the probability that the energy difference between two adjacent energy levels is $\Delta E$, for different amplitudes $\Delta W$ of roughness. Within the framework of nonrelativistic quantum dynamics of Schrödinger billiards, $P(\Delta E)$ follows a Poisson distribution for separable (classically regular) shapes while it should display a Wigner-Dyson [or Gaussian orthogonal ensemble (GOE)] distribution for irregularly shaped (classically chaotic) billiards. Schrödinger billiards refer to the quantum dynamics of a free particle with constant potential inside hard wall boundaries. By contrast, even rectangular shaped Dirac neutrino billiards have been shown to feature a Gaussian unitary ensemble (GUE) distribution because the chiral symmetry found in neutrino billiards breaks time-reversal symmetry.[5] After spectral unfolding [$s=\bar{\rho}(\varepsilon_i)$, with $\langle P(s)\rangle=1$ and $\langle sP(s)\rangle=1$], we find for the ideal rectangular graphene dot ($\Delta W=0$) a near-perfect Poisson distribution [see Fig. 4(a)]. By gradually increasing either the edge roughness or the defect concentration, the distribution smoothly evolves into a Wigner-Dyson-like statistics [see Figs. 4(b) and 4(c)]. Clearly, such a behavior reflects the conservation of time-reversal symmetry in graphene quantum dots. The limiting cases of Poisson and Wigner-Dyson GOE ensembles describe our numerical data very well without the need to resort to ensembles for systems with additional symmetries.[30] We surmise that the reason for this is the breaking of the sublattice symmetry at the edges of the flake. This applies even to the case of $\Delta W=0$, as either A or B type atoms make up the outmost atom of the zigzag edges.[31] As a consequence, properties of neutrino billiards relying on the chiral symmetry do not apply to etched (or cut) graphene islands,[32,33] in agreement with very recent investigations comparing graphene flakes with smooth boundary conditions to flakes terminated by sharp edges.[34] Among the distribution functions suggested for the transition regime for classically mixed phase space,[35–39] we achieved the best fit for the disorder parameters and geometries investigated by using the two-parameter Hasegawa distribution[40]

$$P_H(s;\alpha,\beta) = N\frac{\rho s e^{-\rho s-(\alpha\rho s)^2/2}}{\sqrt{\rho^2 s^2 e^{-\alpha^2\rho^2 s^2}+\beta^2 e^{-2\rho s}}}, \qquad (2)$$

where $\rho$ and $N$ are determined by the normalization conditions $\langle P_H\rangle=\langle sP_H\rangle=1$.[40] While the control parameter $\beta$ describes the transition from Poissonian ($\beta=0$) to Wigner-Dyson statistics ($\beta\to\infty$), $\alpha$ is a system-specific constant. Indeed, we find $\alpha=0.75$ to correctly reproduce our numerically obtained NNSD for different values of both edge roughness as well as scatterers [see Figs. 4(a)–4(c)]. A strong edge roughness of 2 nm (or impurity concentration $n_D=5\times10^{-3}$, $n_C=2\times10^{-2}$) is required to reach the chaotic limit,

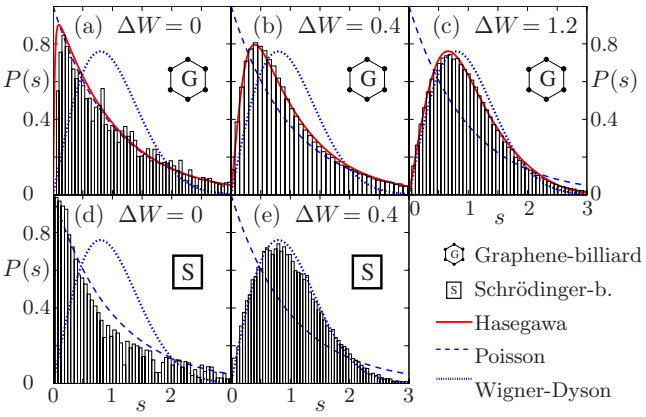


FIG. 4. (Color online) NNSD $P(s)$ of different billiards: rectangular graphene flake with (a) smooth edges ($\beta=0.07$). (b) Finite edge roughnesses $\Delta W=0.4$ nm ($\beta=0.8$) and (c) $\Delta W=1.2$ nm ($\beta=2.5$). [(d) and (e)] Schrödinger billiards with same edge roughness as (a) and (b). The solid curve in (a)–(c) shows fits to the Hasegawa distribution. Dashed (dotted) lines show a Wigner-Dyson (Poisson) statistics as guide to the eye.

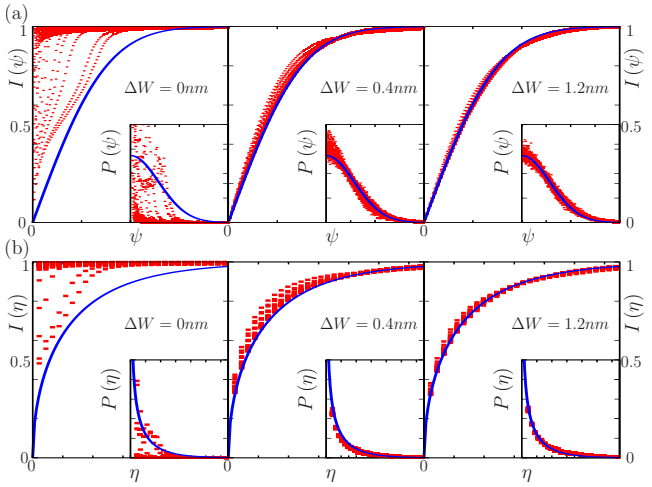


FIG. 5. (Color online) Integrated distribution functions $I(\psi)$ of values (a) $\psi$ [see Eq. (3)] and (b) $\eta$ [see Eq. (4)], for increasing values of edge disorder as labeled in the figures. Each subfigure shows ensemble averages over 50 000 values of $\psi$ for 20 different eigenenergies (corresponding to the different curves). The inset shows the corresponding distributions. The blue solid line shows the RMT predictions for the GOE case (see text).

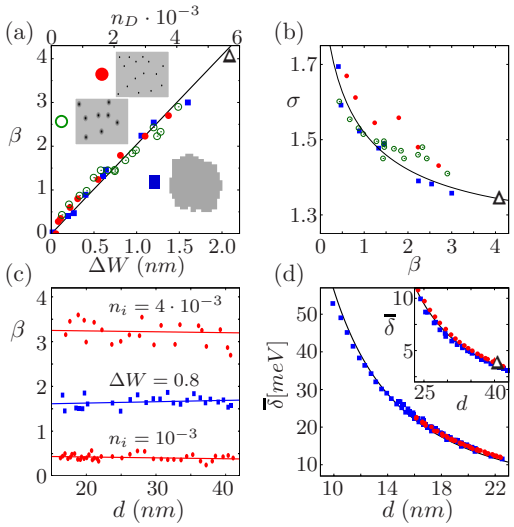


FIG. 6. (Color online) (a) Dependence of the control parameter $\beta$ for the transition from a Poisson to a Wigner-Dyson distribution [Eq. (2)] on the edge roughness amplitude $\Delta W$ (squares), and the density of short-range ($n_D$, full circles) or of long-range ($n_C=4n_D$, rescaled for demonstration purposes only, open circles) impurities. (b) Relation between Hasegawa parameter $\beta$ and second moment $\sigma$ [see Eq. (5)] of the NNSD. (c) Fitted Hasegawa parameter $\beta$ for different dot sizes at three constant disorder strengths as given in the figure. (d) Dependence of rescaled mean-level spacing $\bar{\delta} = \langle \Delta E \cdot E/E_0 \rangle$meV, where $E_0$ was taken at 100 meV, on the size of the quantum dot. Open triangles represent experimental data, rescaled by $\Delta E \to (\Delta E - E_C)\frac{E}{E_0} = (\Delta E - 5)\frac{50}{100}$ to take into account the charging energy $E_C$ and the energy dependence of the DOS (Ref. 6).

i.e., Wigner-Dyson NNSD statistics. For higher disorder concentration, recent results for disordered carbon nanotubes suggest a return to Poisson statistics due to the onset of Anderson localization.[41] Remarkably, for moderate values of the edge roughness amplitude ($\Delta W=0.4$ nm), a Schrödinger and a graphene billiard of the same geometry display a markedly different NNSD (Fig. 4): while the Schrödinger billiard has already reached the Wigner-Dyson limit ($\beta \to \infty$), for the graphene the NNSD still is closer to the Poisson limit, pointing to the unique spectral properties of graphene.

To further elucidate the evolution of the quantum dynamics in graphene-based nanostructures as a function of disorder, we investigate the distribution of eigenstates, i.e., the distribution of values $\psi$ and $\eta := |\psi|^2$. In the GOE limit, the former follows a Gaussian distribution

$$P(\psi) = \frac{1}{\pi} e^{-(\psi^2/\pi)}, \quad I(\psi) = \int_{-\psi}^{\psi} P(\xi) d\xi = \mathrm{erf}\frac{\psi}{\sqrt{\pi}}, \tag{3}$$

while the latter is described by the Porter-Thomas distribution[42]

$$P(\eta) = \frac{1}{\sqrt{2\pi\eta}} e^{-(\eta/2)}, \quad I(\eta) = \mathrm{erf}\sqrt{\frac{\eta}{2}}, \tag{4}$$

originally suggested to describe the distribution of resonance widths (i.e., transition probabilities) in nuclear reactions. For graphene billiards, we find a slow convergence toward the random matrix theory (RMT) predictions for the GOE ensemble in the distributions for $\psi$ [see Fig. 5(a)] and $\eta$ [see Fig. 5(b)], in line with the slow convergence of the NNSD to the GOE limit.

The reason for the increased stability of graphene-based devices against transition to the GOE limit is closely related to the electronic structure of graphene at the $K$ points [Fig. 1(a)]. In a classical rectangular ballistic billiard with only rectangular edges [Figs. 1 and 4(d)], an additional constant of motion, the magnitude of the linear momentum $|\mathbf{k}|$, exists. Such billiards are therefore classically (pseudo) integrable,[43] and do not feature chaotic dynamics irrespective of the number or size of the edges. Consequently, Schrödinger billiards in the limit of small deBroglie wavelength feature pseudo-Poissonian statistics. By contrast, for wave numbers near the $\Gamma$ point, the large wavelength cannot resolve the exactly rectangularly shaped edges, and tend toward the Wigner-Dyson statistics. For the same size of the edges $\Delta W$, the graphene eigenstate features a much shorter wavelength due to the position of the Dirac cone near the $K$ point in the Brillouin zone. The quantum dynamics of the graphene billiard is therefore closer to the classical limit and its level statistics closer to the Poisson limit of regular dynamics.

Of potential technological significance is the dependence of the NNSD on the disorder in graphene billiards which might be used as a quantitative indicator of its strength. For all three classes of disorder (edge roughness, short-range, and long-range disorders), we find a linear relation between the NNSD parameter $\beta$ and the edge roughness amplitude, $\beta \approx 2\Delta W$, and between $\beta$ and the density of short-range $\beta \approx 0.7 n_D$, as well as long-range defects $\beta \approx 0.2 n_C$ [Fig. 6(a)]. As $\beta$ can be obtained with high precision from a fit to $P(s)$, the edge roughness or defect density can be deduced from the NNSD if the distribution is (approximately) Poisson-type in the limit $\Delta W=0$ ($n_D=0$). We suggest that this dependence

could be used to estimate the disorder in experimentally realized regularly shaped phase-coherent graphene quantum dots. Numerically, we find $\beta \approx 4$ in a fit to data from recent experimental investigations of a 40 nm graphene billiard,[6] corresponding to an effective roughness $\Delta W_e \approx 2$ nm, or an effective (short-range) defect rate $n_D \approx 5.5 \times 10^{-3}$ (see black triangles in Fig. 6). As the second moment,

$$\sigma = \langle s^2 P(s) \rangle_\xi, \tag{5}$$

of the NNSD decreases with increasing disorder, one could alternatively obtain an estimate for the roughness of a flake from $\sigma$. We find, however, that the dependence on $\beta$ is more reliable, as the entire distribution is used for a fit to $P_H$ [see Fig. 6(b)].

While the shape of the unfolded NNSD, $P(s)$, is sensitively dependent on disorder, it is, to a good degree of approximation, size independent, as our numerical data confirm [see Fig. 6(c)]. Note that the normalization $\langle sP(s) \rangle = 1$ scales out size-related effects. By contrast, the absolute level spacing $\langle \Delta E \rangle$ contains direct information on the size of quantum confinement. By rescaling each level spacing by the local energy, relative to a fixed energy $E_0 = 100$ meV, one obtains the size dependent (but almost energy independent) expectation value

$$\bar{\delta} = \left\langle \Delta E \frac{E}{E_0} \right\rangle = (\hbar v_F)^2 \frac{2}{d^2 E_0} = \frac{5500 \text{ nm}^2}{d^2} \text{ meV}. \tag{6}$$

This rescaled mean-level spacing is, indeed, independent of edge roughness and disorder [see Fig. 6(d)]. Note that, in spite of the large contribution of localized states near the Fermi edge, the mean-level spacing accurately follows Eq. (6). To achieve agreement with Eq. (6) we have included in the ensemble the states up to 1 eV away from the Fermi edge. The increased spacing of the more distant levels offsets the clustering of the localized levels near the Fermi edge. Agreement with the experimental data[6] for $d = 40$ nm is surprisingly good.

## V. CONCLUSIONS

In conclusion, the spectrum of realistic graphene quantum dots in the presence of disorder (edge roughness or defects) reveal unique features which differ from both Schrödinger or Dirac billiards of confined massive or massless free particles. The graphene band structure near the $K$ points leaves clear imprints. They include interference structures in the wave functions, enhanced confinement effects, and a delayed transition from Poisson to Wigner-Dyson nearest-neighbor distributions. While one still "cannot hear the imperfect shape of the drum," the size and roughness of graphene quantum dots can be, indeed, inferred from the spectral properties.

## ACKNOWLEDGMENTS

We thank K. Ensslin, T. Ihn, S. Rotter, and L. Wirtz for valuable discussions. F.L. and J.B. acknowledge support from the FWF-SFB Adlis while C.S. acknowledges support from NCCR.

[1] K. S. Novoselov, A. K. Geim, S. V. Morozov, D. Jiang, M. I. Katsnelson, I. V. Grigorieva, S. V. Dubonos, and A. A. Firsov, Nature (London) **438**, 197 (2005).
[2] Y. Zhang, Y.-W. Tan, H. L. Stormer, and P. Kim, Nature (London) **438**, 201 (2005).
[3] A. K. Geim and K. S. Novoselov, Nature Mater. **6**, 183 (2007).
[4] B. Trauzettel, D. V. Bulaev, D. Loss, and G. Burkard, Nat. Phys. **3**, 192 (2007).
[5] M. V. Berry and R. J. Mondragon, Proc. R. Soc. London **A412**, 53 (1987).
[6] L. A. Ponomarenko, F. Schedin, M. I. Katsnelson, R. Yang, E. H. Hill, K. S. Novoselov, and A. K. Geim, Science **320**, 356 (2008).
[7] H.-J. Stöckmann, *Quantum Chaos* (Cambridge University Press, Cambridge, 1999).
[8] H. Min, J. E. Hill, N. A. Sinitsyn, B. R. Sahu, L. Kleinman, and A. H. MacDonald, Phys. Rev. B **74**, 165310 (2006).
[9] N. Tombros, C. Jozsa, M. Popinciuc, H. T. Jonkman, and B. J. van Wees, Nature (London) **448**, 571 (2007).
[10] D. Huertas-Hernando, F. Guinea, and A. Brataas, Phys. Rev. B **74**, 155426 (2006).
[11] M. I. Katsnelson, K. S. Novoselov, and A. K. Geim, Nat. Phys. **2**, 620 (2006).
[12] N. Dombay and A. Calogeracos, Phys. Rep. **315**, 41 (1999).
[13] M. Y. Han, B. Özyilmaz, Y. Zhang, and P. Kim, Phys. Rev. Lett. **98**, 206805 (2007).
[14] Z. Chen, Y. Lin, M. Rooks, and P. Avouris, Physica E (Amsterdam) **40**, 228 (2007).
[15] Y.-M. Lin, V. Perebeinos, Z. Chen, and P. Avouris, Phys. Rev. B **78**, 161409(R) (2008).
[16] K. Todd, H.-T. Chou, S. Amasha, and D. Goldhaber-Gordon, Nano Lett. **9**, 416 (2009).
[17] F. Molitor, A. Jacobsen, C. Stampfer, J. Güttinger, T. Ihn, and K. Ensslin, Phys. Rev. B **79**, 075426 (2009).
[18] X. Liu, J. B. Oostinga, A. F. Morpurgo, and L. M. K. Vandersypen, arXiv:0812.4038 (unpublished).
[19] F. Miao, S. Wijeratne, Y. Zhang, U. C. Coskun, W. Bao, and C. N. Lau, Science **317**, 1530 (2007).
[20] C. Stampfer, J. Güttinger, F. Molitor, D. Graf, T. Ihn, and K. Ensslin, Appl. Phys. Lett. **92**, 012102 (2008).
[21] C. Stampfer, E. Schurtenberger, F. Molitor, J. Güttinger, T. Ihn, and K. Ensslin, Nano Lett. **8**, 2378 (2008).
[22] S. Schnez, F. Molitor, C. Stampfer, J. Güttinger, I. Shorubalko, T. Ihn, and K. Ensslin, Appl. Phys. Lett. **94**, 012107 (2009).
[23] J.-H. Chen, C. Jang, S. Adam, M. S. Fuhrer, E. D. Williams, and M. Ishigami, Nat. Phys. **4**, 377 (2008).
[24] C. Lanczos, J. Res. Natl. Bur. Stand. **45**, 255 (1950).
[25] S. Reich, J. Maultzsch, C. Thomsen, and P. Ordejon, Phys. Rev. B **66**, 035412 (2002).
[26] Y.-W. Son, M. L. Cohen, and S. G. Louie, Phys. Rev. Lett. **97**, 216803 (2006).
[27] N. M. R. Peres, A. H. Castro Neto, and F. Guinea, Phys Rev. B

**73**, 195411 (2006); D. Gunlycke, D. A. Areshkin, and C. T. White, Appl. Phys. Lett. **90**, 142104 (2007); J. Fernandez-Rossier, J. J. Palacios, and L. Brey, Phys. Rev. B **75**, 205441 (2007).

[28] M. Fujita, K. Wakabayashi, K. Nakada, and K. Kusakabe, J. Phys. Soc. Jpn. **65**, 1920 (1996).

[29] M. Evaldsson, I. V. Zozoulenko, H. Xu, and T. Heinzel, Phys. Rev. B **78**, 161407(R) (2008).

[30] A. Altland and M. R. Zirnbauer, Phys. Rev. Lett. **76**, 3420 (1996).

[31] Here, A and B refer to the two sublattices of the honeycomblike hexagonal graphene carbon lattice.

[32] P. Recher, J. Nilsson, G. Burkard, and B. Trauzettel, Phys. Rev. B **79**, 085407 (2009).

[33] S. Schnez, K. Ensslin, M. Sigrist, and T. Ihn, Phys. Rev. B **78**, 195427 (2008).

[34] J. Wurm, A. Rycerz, I. Adagideli, M. Wimmer, K. Richter, and H. U. Baranger, Phys. Rev. Lett. **102**, 056806 (2009).

[35] T. A. Brody, Lett. Nuovo Cimento Soc. Ital. Fis. **7**, 482 (1973).

[36] E. Caurier, B. Grammaticos, and A. Ramani, J. Phys. A **23**, 4903 (1990).

[37] F. M. Izrailev, Phys. Lett. A **134**, 13 (1988).

[38] G. Lenz and F. Haake, Phys. Rev. Lett. **67**, 1 (1991).

[39] M. V. Berry and M. Robnik, J. Phys. A **17**, 2413 (1984).

[40] H. Hasegawa, H. J. Mikeska, and H. Frahm, Phys. Rev. A **38**, 395 (1988).

[41] I. Amanatidis and S. N. Evangelou, arXiv:0806.4884 (unpublished).

[42] C. E. Porter and R. G. Thomas, Phys. Rev. **104**, 483 (1956).

[43] P. J. Richens and M. V. Berry, Physica D **2**, 495 (1981).